

Analysis of unavoidable geometric errors in the side wall of end-milled parts for corner surface[†]

Kun Sang Lee and Kang Kim*

School of Mechanical and Automotive Engineering, Kookmin University, Seoul, 136-702, Korea

(Manuscript Received October 6, 2008; Revised November 15, 2008; Accepted November 24, 2008)

Abstract

The location and the size of a geometrically defected region in the side wall of a corner, which is generated during the flat end-milling process, are investigated through experiments and geometrical analysis. A corner with inner and outer surfaces is assumed to be made up of one arc-surface patch and two flat-surface patches. Based on the previous findings that the change of material removal per tooth affects the geometry of the end-milled side wall, it is expected that the geometrically defected regions are located around the corner when the tool is approaching and leaving the arc surface. In this respect, analytic models are proposed to predict the location and the size of a geometrically defected region, which are then validated via comparison with the experimental results.

Keywords: End-milling process; Geometric errors of side wall; Corner surface; Cutting conditions; Material removal per tooth

1. Introduction

There is no question on the importance of mold and die in mass production. For example, the quality and the cost of injection molding parts are affected by the mold. The general 3-D part shape is represented as a combination of flat-surface and arc-surface patches. As a result, the end-milling process is commonly used for making a mold even though there are several conventional and non-conventional manufacturing processes. The time and money for the finishing operations, which are inevitable in mold making, are dependent on the geometrical accuracy of the mold surface just before the finishing process. It is thus required to understand the geometric characteristics of the end-milled surface. Many attempts have been made to examine the relationships between the geometric features of milled surfaces and the independent cutting variables in the machining system [1-7]. The

effect of the elastic deflection of a tool during end-milling on the surface integrity of a part has been also investigated [8-11]. Furthermore, geometric characteristics of the end-milled flat surface and cylindrical surface were studied previously [12,13].

In this paper, analytic models, which reveal the location and the size of the geometrically defected end-milled corner surface, are developed. Proposed models are subsequently validated by comparing analytically the simulated surface with the experimentally end-milled surface under the same cutting conditions.

2. Defect zone length, valley angle and valley depth

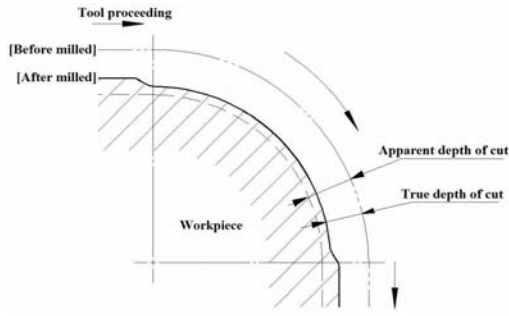
The exaggerated typical profiles of the end-milled outer and inner corner surfaces are given in Figs. 1(a) and (b), respectively, showing two distinctive characteristics. One is that the true depth of cut on the arc-surface region is either larger in case of the outer corner or smaller for the inner corner than the true depth of cut on the flat-surface region, even if the feed rate and the apparent depth of cut are kept constant during

[†] This paper was recommended for publication in revised form by Associate Editor Dae-Eun Kim

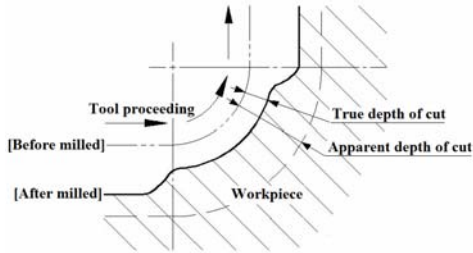
* Corresponding author. Tel.: +82 2 910 4676, Fax.: +82 2 910 4839

E-mail address: kangkim@kookmin.ac.kr

© KSME & Springer 2009



(a) Outer corner

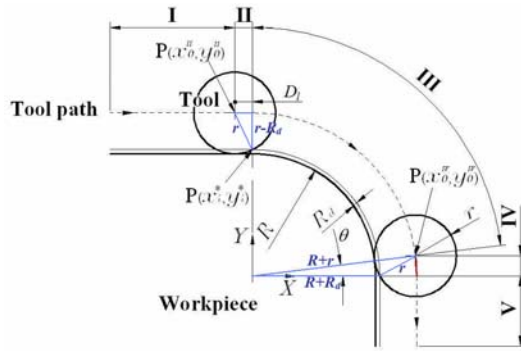


(b) Inner corner

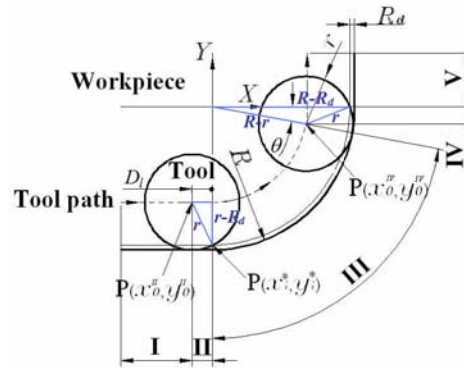
Fig. 1. Typical profile of end-milled corner surface (exaggerated presentation).

the process. Another is that gradual changes in true depth of cut occur just before entering and leaving the arc-surface region. Each portion, which shows the gradual change in true depth of cut, is named as 'defect zone'. As a result, the corner surface always has two defect zones. To maintain the consistency in terminology with the previous work [12, 13], the range and the relative depth of the defect zone formed just before entering the arc-surface region are characterized with the help of 'defect zone length (D_d)' and 'valley depth (V_d)'. Similarly, the defect zone shaped just before leaving the arc-surface region is characterized by 'valley angle (θ)' and 'valley depth (V_d)'. The defect zone length and the valley angle are depicted in Fig. 2.

Fig. 2 is a schematic illustration of the relative motion of the end-milling tool in the process. If the spindle speed, the feed rate and the apparent depth of cut are kept constant during the process, the material removal per tooth is also constant in region I, followed by gradual changes from this constant value to a certain one in region II. It is then maintained for some duration of time in region III, and changes back into the first constant value in region IV. Finally, it is



(a) Outer corner



(b) Inner corner

Fig. 2. Classification of regions according to surface geometry.

kept constant as the first constant value in region V. From this point of view, the corner surface can be regarded as a composition of five regions. For convenience, they are named 'steady cutting region in flat-surface' (I and V in Fig. 2), 'entry region' (II in Fig. 2), 'steady cutting region in arc-surface' (III in Fig. 2) and 'exit region' (IV in Fig. 2), respectively. Each region is defined as a location of the tool center.

3. Experiment

Fig. 3 illustrates the shape and size of specimens, made from general purpose carbon steel, (SM45C). The CNC vertical milling machine used in the experiment was a Model TMV-40M. Prior to the experiment, the machine table movement errors were measured and calibrated, so that the errors were kept to less than $0.5\mu\text{m}$. Titanium-coated standard 2 flutes high speed steel end-milling tools were used for the experiment. The diameter and the helix angle of tools

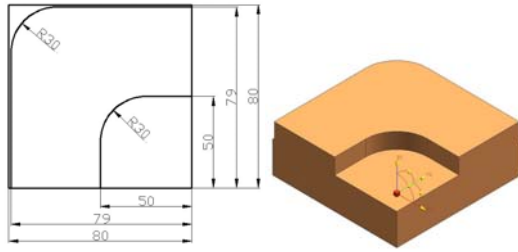


Fig. 3. Specimen. (No scale, unit: mm).

are 20mm and 30°, respectively. Table 1 shows the experimental cutting conditions. The spindle speed, the feed rate and the axial depth of cut were set equal to 381 rev/min, 70 mm/min and 10mm, respectively. The radial depth of cut was varied from 0.5mm to 1.5mm. As expected, the surfaces corresponding to the regions II and IV were geometrically inaccurate compared with the surfaces of the other regions. To obtain a more precise profile of the specimen, only the regions II and IV were measured by Form Tallysurf Series 2 system.

4. Defect zone modeling

It has been recognized that there is an intimate relationship between the change of material removal per tooth during the process and the defect zone, which arises from the machining elasticity phenomenon [12, 13]. As mentioned, the defect zone length, the valley angle and the valley depth are introduced to develop analytic models. The ranges of the defect zones in regions II and IV are presumed from the models for the defect zone length and the valley angle, respectively. The valley depth, which signifies the relative difference between the after-machined surface in radial direction and a reference surface, is assumed to be proportional to the change of the material removal per tooth. Via the comparison between the experimental results and the simulation ones obtained by using the valley depth model, the proportional factor can be found.

4.1 Defect zone length and valley angle

Because the tool radius is not zero, the material removal rate on the corner surface is not equal to that on the straight surface even if the feed rate of tool center and the apparent depth of cut are kept constant. Therefore, the existence of a geometrically defected region on the surface is inevitable around which the

Table 1. Experimental conditions.

Cut conditions	Value
Feed rate (mm/min)	70
Spindle speed (rpm)	381
Axial depth of cut (A_d) (mm)	10
Apparent radial depth of cut (R_d) (mm)	0.5, 1.0, 1.5
Feed per tooth (mm/tooth)	0.09
Tool diameter (mm)	20
Tool path	down cut milling
Tool revolution direction	clockwise

surface patches with two different curvatures meet.

Figure 2 shows the coordinate system and the tool location at the instant of occurrence of the change in the material removal per tooth. The origin of coordinate coincides with the arc center of the after-machined surface. It is assumed that the X and Y axes are passing through the final point and the initial point of the arc in the order of surface generation, respectively. The point $P(x_0^{II}, y_0^{II})$ indicates the tool center location when its periphery meets the crossing point of before-machined corner surface and Y axis. The change in the material removal per tooth starts when the tool center is located at $P(x_0^{II}, y_0^{II})$, and continues until the tool center meets the Y axis. Thus, the defect zone length, D_l , is equal to the distance between $P(x_0^{II}, y_0^{II})$ and $P(0, y_0^{II})$. The coordinate of $P(x_0^{II}, y_0^{II})$ satisfies the following set of equations:

$$(x_0^{II})^2 + \{y_0^{II} - (-1)^m (R + v)\}^2 = r^2 \quad (x_0^{II} < 0) \quad (1)$$

$$y_0^{II} = (-1)^m (R + \delta) \quad (2)$$

$$\begin{cases} m=0, & \delta=r, & v=R_d & (\text{outercorner}) \\ m=1, & \delta=-r, & v=-R_d, & (\text{innercorner}) \end{cases}$$

where R is the after-machined corner radius; r is the tool radius; R_d is the apparent radial depth of cut; m , δ and v are dummy variables. As a result, the defect zone length, D_l , can be expressed as

$$D_l = |x_0^{II}| = \sqrt{R_d(2r - R_d)} \quad (3)$$

Similarly, the tool traveling along the circular path meets the crossing point of before-machined corner surface and X axis when the tool center is located at $P(x_0^{IV}, y_0^{IV})$. The material removal per tooth is changing from this instance, and arrives at another constant value when the tool center reaches the X axis. The angle between the X axis and the line connecting

$P(x_0^{IV}, y_0^{IV})$ and the origin corresponds to the valley angle, θ . The values of x_0^{IV} and y_0^{IV} , which are required to obtain θ , can be found from an intersection point of the following two circles given by:

$$(x_0^{IV})^2 + (y_0^{IV})^2 = (R + \delta)^2 \tag{4}$$

$$\left\{ x_0^{IV} - (R + \nu) \right\}^2 + (y_0^{IV})^2 = \delta^2 \tag{5}$$

$$\left[\begin{array}{l} x_0^{IV} > 0, \quad y_0^{IV} > 0 \quad (\text{outer corner}) \\ x_0^{IV} > 0, \quad y_0^{IV} < 0 \quad (\text{inner corner}) \end{array} \right]$$

The valley angle, θ , can be expressed as follows:

$$\theta = \tan^{-1} \left| \frac{y_0^{IV}}{x_0^{IV}} \right| \quad (0 < \theta < \frac{\pi}{2}) \tag{6}$$

4.2 Material removal per tooth in region II

The material removal per tooth is defined to be the amount of workpiece material removed by a cutting tooth when the tool moves the distance that is equal to the feed per tooth, f_t . It is determined from the equation

$$f_t = \frac{F}{N \times Z} \tag{7}$$

where F is the feed speed of the workpiece, N is the rotational speed of the tool and Z is the number of teeth on the tool periphery. If the displacement of the tool center is equal to the defect zone length, the total number of the material removal by every cutting tooth, n , is

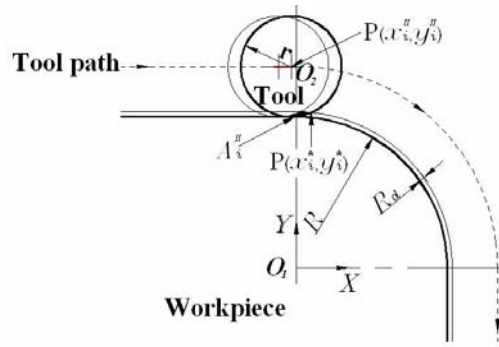
$$n = INT \{ D_i / f_t \} \tag{8}$$

If the tool center is located at $P(x_i^{II}, y_i^{II})$ when the i^{th} material removal occurs in the region II, x_i^{II} and y_i^{II} in Figs. 4 (a) and (b) are expressed as

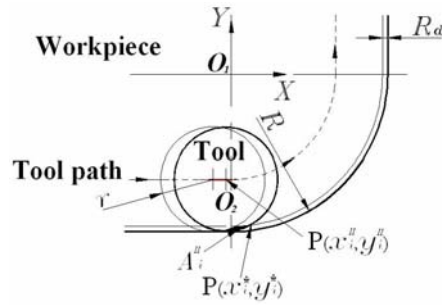
$$x_i^{II} = x_0^{II} + i \times f_t \quad (i = 1, 2, \dots, n) \tag{9}$$

$$y_i^{II} = (-1)^m (R + \delta) \tag{10}$$

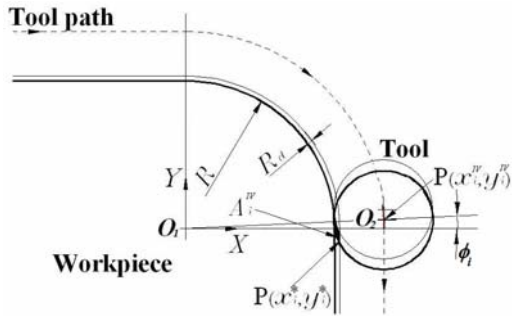
A point, $P(x_i^*, y_i^*)$, is the location of contact between the tool and the workpiece surface at that very instant. Thus, x_i^* and y_i^* must satisfy the following set of equations:



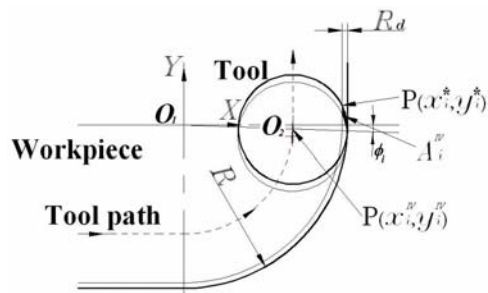
(a) Outer corner (region II)



(b) Inner corner (region II)



(c) Outer corner (region IV)



(d) Inner corner (region IV)

Fig. 4. Coordinate system for valley depth analysis.

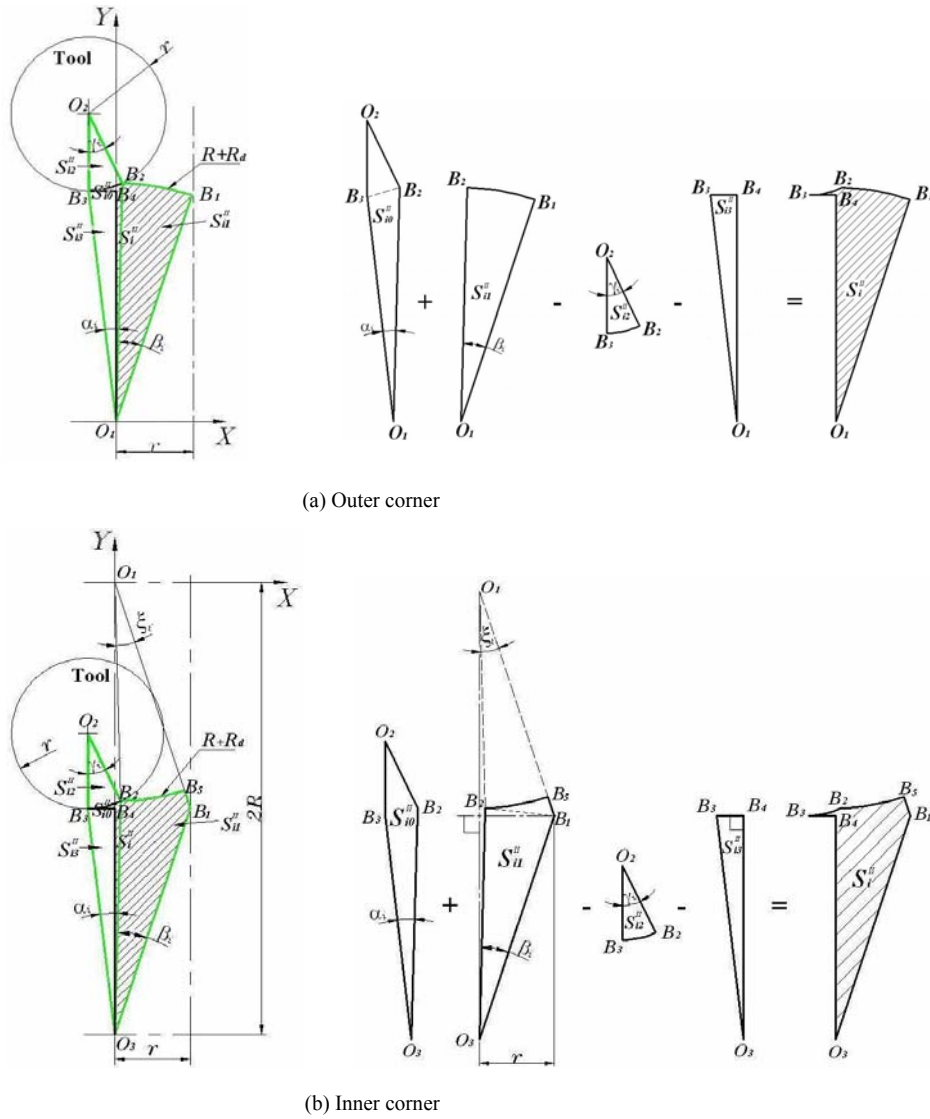


Fig. 5. Area S_i'' after the i^{th} removal in region II.

$$(x_i^* - x_i'')^2 + (y_i^* - y_i'')^2 = \delta^2 \quad (i=0,1,2,\dots,n) \quad (11)$$

$$(x_i^*)^2 + (y_i^*)^2 = (R+v)^2 \quad (12)$$

$$\begin{cases} x_i^* \geq 0, & y_i^* \geq 0 & (\text{outercorner}) \\ x_i^* \geq 0, & y_i^* \leq 0 & (\text{innercorner}) \end{cases}$$

To find the i^{th} material removal per tooth, an area, S_i'' , is introduced. As shown in Fig. 5, S_i'' can be expressed as a function of sub-areas, S_{i0}'' , S_{i1}'' , S_{i2}'' and S_{i3}'' . Figure 5 (a) shows these sub-areas and points for the case of outer corner. The sub-areas are defined by points, O_1 , O_2 , B_1 , B_2 , B_3 and B_4 . The

points O_1 and O_2 are the center of arc ($P(0,0)$) and the tool center ($P(x_i'', y_i'')$). The coordinate of B_1 is an intersection of the before-machined arc-surface and the line $X=r$, is $P(r, (R+R_d)\sin\{\cos^{-1}(r/(R+R_d))\})$; the coordinate of B_2 is $P(x_i^*, y_i^*)$; the coordinate of B_3 is an intersection of the after-machined flat-surface and the line $X=x_i''$, is $P(x_i'', R)$; the coordinate of B_4 is an intersection of the Y axis and the line $Y=R$, is $P(0, R)$. Therefore, the angles α_i ($\angle B_2O_1B_3$), β_i ($\angle B_1O_1B_2$) and γ_i ($\angle B_2O_2B_3$) can be written as

$$\alpha_i = \tan^{-1} \left| \frac{x_i^*}{y_i^*} \right| + \tan^{-1} \left| \frac{x_i''}{R} \right| \quad (13)$$

$$\beta_i = \sin^{-1} \left| \frac{r}{R + R_d} - \tan^{-1} \left| \frac{x_i^*}{y_i^*} \right| \right| \quad (14)$$

$$\gamma_i = \sin^{-1} \left| \frac{x_i^* - x_i^{II}}{r} \right| \quad (15)$$

The sub-areas, S_{i0}^{II} (the area of polygon $O_1B_2O_2B_3$), S_{i1}^{II} (the area of sector $O_1B_1B_2$), S_{i2}^{II} (the area of sector $O_2B_2B_3$) and S_{i3}^{II} (the area of triangle $O_1B_3B_4$) are also written as

$$S_{i0}^{II} = \frac{1}{2} \left\{ r(x_i^* - x_i^{II}) + \sqrt{(x_i^{II})^2 + R^2} \sqrt{(x_i^*)^2 + (y_i^*)^2} \sin \alpha_i \right\} \quad (16)$$

$$S_{i1}^{II} = \frac{1}{2} (R + R_d)^2 \beta_i \quad (17)$$

$$S_{i2}^{II} = \frac{1}{2} r^2 \gamma_i \quad (18)$$

$$S_{i3}^{II} = \frac{1}{2} |R \times x_i^{II}| \quad (19)$$

The sub-areas and points for the inner corner case are depicted in Fig. 5 (b). For this case, a pseudo center, O_3 , with its coordinate $P(0, -2R)$, is introduced. The coordinates of the fixed points for B_1 and B_4 are $P(r, -R)$ and $P(0, -R)$, respectively, while the coordinates of the points, B_2 and B_3 , corresponding to the initial and the final contact points between the cutting edge and the workpiece surface in the i^{th} material removal per tooth, are $P(x_i^*, y_i^*)$ and $P(x_i^{II}, -R)$. Even though the definitions of α_i ($\angle B_2O_3B_3$), S_{i0}^{II} (the area of polygon $O_2B_2O_3B_3$) and S_{i3}^{II} (the area of triangle $O_3B_3B_4$) are different from those in the outer corner case, equations (13), (16) and (19) are still valid. There are no changes in the definitions of the γ_i ($\angle B_2O_2B_3$) and S_{i2}^{II} (the area of sector $O_2B_2B_3$) compared to the outer corner case. The newly defined β_i ($\angle B_1O_3B_2$), ξ_i ($\angle B_1O_1B_2$) and S_{i1}^{II} (the area of polygon $O_1B_1O_3B_2$ - the area of sector $O_1B_1B_2$) can be written as

$$\beta_i = \tan^{-1} \left| \frac{r}{R} \right| - \tan^{-1} \left| \frac{x_i^*}{2R + y_i^*} \right| \quad (20)$$

$$\xi_i = \tan^{-1} \left| \frac{r}{R} \right| - \tan^{-1} \left| \frac{x_i^*}{y_i^*} \right| \quad (21)$$

$$S_{i1}^{II} = \frac{1}{2} \left[\sqrt{R^2 + r^2} \left\{ \sqrt{(x_i^*)^2 + (y_i^* + 2R)^2} \sin \beta_i + \sqrt{(x_i^*)^2 + (y_i^*)^2} \sin \xi_i \right\} - (R - R_d)^2 \xi_i \right] \quad (22)$$

Therefore, the area, S_i^{II} , is given by:

$$S_i^{II} = S_{i0}^{II} + S_{i1}^{II} - S_{i2}^{II} - S_{i3}^{II} \quad (23)$$

And each sub-area for the outer corner case can be found in Eqs. (16)-(19). On the other hand, for the inner corner case, Eqs. (16), (23), (18) and (19) are available.

In consequence, the material removal per tooth at the i^{th} occurrence in the region II can be expressed as

$$A_i^{II} = S_{i-1}^{II} - S_i^{II} \quad (i = 1, 2, \dots, n) \quad (24)$$

and the initial value of the material removal per tooth, A_0^{II} , is equal to the material removal per tooth in the region I. It can readily be obtained as a function of the feed per tooth and the apparent depth of cut in this region as:

$$A_0^{II} = |f_t \times R_d| \quad (25)$$

4.3 Material removal per tooth in region IV

If the angular displacement of the tool center corresponding to the feed per tooth in the valley is θ_i , it is given by

$$\theta_i = \frac{F}{ZN \times (R + \delta)} \quad (26)$$

The total number of the material removal by every cutting tooth in the valley, n , is

$$n = INT \{ \theta / \theta_i \} \quad (27)$$

such that when the i^{th} material removal occurs in the valley, the angular displacement of the tool center, ϕ_i , and the coordinate of tool center, $P(x_i^{IV}, y_i^{IV})$ in Figs. 4(c) and (d) can be expressed as

$$\phi_i = \theta - (i \times \theta_i) \quad (i = 1, 2, \dots, n) \quad (28)$$

$$x_i^{IV} = (R + \delta) \cos \phi_i \quad (29)$$

$$y_i^{IV} = (-1)^m (R + \delta) \sin \phi_i \quad (30)$$

If the point of contact between the tool and the workpiece surface is $P(x_i^*, y_i^*)$ at this moment, x_i^* and y_i^* must satisfy the following set of equations:

$$x_i^* = R + v \quad (i = 0, 1, 2, \dots, n) \quad (31)$$

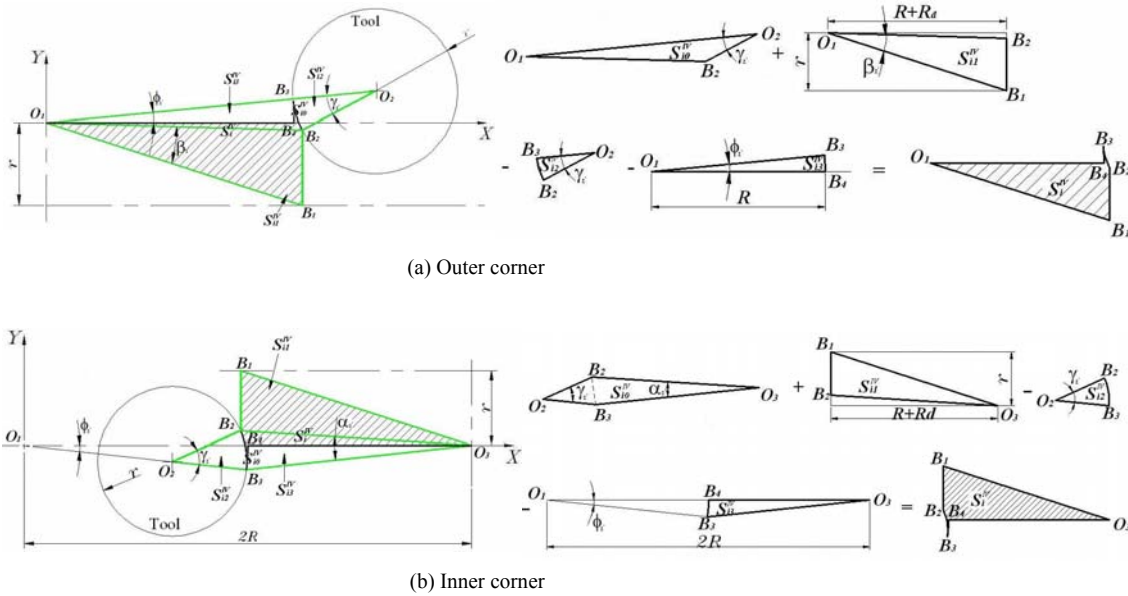


Fig. 6. Area S_i^{IV} after the i^{th} removal in region IV.

$$\begin{aligned} (x_i^* - x_i^{IV})^2 + (y_i^* - y_i^{IV})^2 &= \delta^2 \\ \begin{cases} y_i^* \leq 0 & (\text{outer corner}) \\ y_i^* \geq 0 & (\text{inner corner}) \end{cases} \end{aligned} \quad (32)$$

As shown in Fig. 6, an area, S_i^{IV} , and sub-areas, S_{i0}^{IV} , S_{i1}^{IV} , S_{i2}^{IV} and S_{i3}^{IV} , are introduced to find the i^{th} material removal per tooth in region IV. The points, which are used to describe the sub-areas for the case of outer corner, are shown in Fig. 6(a). The points O_1 and O_2 are the center of arc ($P(0,0)$) and the tool center ($P(x_i^{IV}, y_i^{IV})$), respectively. In this case, the coordinate of B_1 , which is an intersection of the before-machined flat-surface and the line $Y=-r$, is $P(x_i^*, -r)$; the coordinate of B_2 is $P(x_i^*, y_i^*)$; the coordinate of B_3 , which is an intersection of the after-machined arc-surface and the line $\overline{O_1O_2}$, is $P(x_i^{IV} \times R / (R+r), y_i^{IV} \times R / (R+r))$; the coordinate of B_4 is $P(R, 0)$. The angle, ϕ , is given by equation (28) and the angles γ_i ($\angle B_2O_2B_3$) can be written as

$$\gamma_i = \frac{\pi}{2} - \tan^{-1} \left| \frac{y_i^{IV}}{x_i^{IV}} \right| - \tan^{-1} \left| \frac{x_i^{IV} - x_i^*}{y_i^{IV} - y_i^*} \right| \quad (33)$$

The sub-areas, S_{i0}^{IV} (the area of triangle $O_1O_2B_2$), S_{i1}^{IV} (the area of triangle $O_1B_1B_2$), S_{i2}^{IV} (the area of sector $O_2B_2B_3$) and S_{i3}^{IV} (the area of sector $O_1B_3B_4$), are expressed in the form of following equations:

$$S_{i0}^{IV} = \frac{1}{2} (R+r) \times r \sin \gamma_i \quad (34)$$

$$S_{i1}^{IV} = \frac{1}{2} (R+R_d)(r+y_i^*) \quad (35)$$

$$S_{i2}^{IV} = \frac{1}{2} r^2 \gamma_i \quad (36)$$

$$S_{i3}^{IV} = \frac{1}{2} R^2 \phi_i \quad (37)$$

The sub-areas and points for the inner corner case are also depicted in Fig. 6(b). The pseudo center, O_3 , and the fixed points, B_1 and B_4 , are located at $(2R, 0)$, (x_i^*, r) and $(R, 0)$, respectively. The coordinates of the points, B_2 and B_3 , which correspond to the initial and the final contact points between the cutting edge and the workpiece surface in the i^{th} material removal per tooth, are $P(x_i^*, y_i^*)$ and $P(x_i^{IV} \times R / (R-r), y_i^{IV} \times R / (R-r))$. Hence, the angles, α_i ($\angle B_2O_3B_3$) and γ_i ($\angle B_2O_2B_3$) can be written as

$$\alpha_i = \tan^{-1} \left| \frac{y_i^*}{2R-x_i^*} \right| + \tan^{-1} \left| \frac{y_i^{IV} \{R/(R-r)\}}{2R-x_i^{IV} \{R/(R-r)\}} \right| \quad (38)$$

$$\gamma_i = \tan^{-1} \left| \frac{y_i^{IV}}{x_i^{IV}} \right| + \tan^{-1} \left| \frac{y_i^{IV} - y_i^*}{x_i^{IV} - x_i^*} \right| \quad (39)$$

In this case, the definition and equation of S_{i2}^{IV} (the area of sector $O_2B_2B_3$) are identical to those for outer corner. The other sub-areas, S_{i0}^{IV} (the area of poly-

gon $O_2B_2O_3B_3$), S_{i1}^{IV} (the area of triangle $O_3B_1B_2$) and S_{i3}^{IV} (the area of triangle $O_1B_3O_3$ - the area of sector $O_1B_3B_4$), are also expressed:

$$S_{i0}^{IV} = \frac{1}{2}r^2 \times \sin \gamma_i + \sin \alpha_i \left(\sqrt{(2R - x_i^*)^2 + (y_i^*)^2} \times \sqrt{[2R - x_i^{IV}\{R/(R-r)\}]^2 + [y_i^{IV}\{R/(R-r)\}]^2} \right) \quad (40)$$

$$S_{i1}^{IV} = \frac{1}{2}(R + R_d)(r - y_i^*) \quad (41)$$

$$S_{i3}^{IV} = R^2 \left(\sin \phi_i - \frac{1}{2}\phi_i \right) \quad (42)$$

Therefore, the area, S_i^{IV} , can be written as:

$$S_i^{IV} = S_{i0}^{IV} + S_{i1}^{IV} - S_{i2}^{IV} - S_{i3}^{IV} \quad (43)$$

Each sub-area for the outer corner can be found in Eqs. (34)-(37). For the case of inner corner, Eqs. (36) and (40)-(42) are available.

In consequence, the material removal per tooth at the i^{th} occurrence in the region IV can be expressed as

$$A_i^{IV} = S_i^{IV} - S_{i-1}^{IV} \quad (i = 1, 2, \dots, n) \quad (44)$$

and the initial value of the material removal per tooth, A_0^{IV} , is equal to the material removal per tooth in the region III. It can readily be obtained as a function of θ and the radial depth of cut in this region such that

$$A_0^{IV} = \frac{|v|}{2} \times (2R + v) \times \theta_i \quad (45)$$

4.4 Valley depth

The apparent depth of cut is usually greater than the true depth of cut. If the difference between the two depths is larger, the defect zone depth appears to be deeper. This has been known as 'machining elasticity'. For the application of the machining elasticity concept, a coefficient of machining elasticity, K , is defined by the ratio of true depth of cut to material removal per tooth as

$$K = \frac{T_0}{A_0} = \frac{T_i}{A_i} \quad (46)$$

where T_0 is the initial value of the true depth of cut equal to the true depth of cut in the steady cutting region, T_i is the true depth of cut at the i^{th} occurrence in the defect zone, and A_0 and A_i are the values of the

material removal per tooth in the steady cutting region and at the i^{th} occurrence in the defect zone, respectively. Thus, the valley depth at the i^{th} occurrence in the defect zone, $(V_d)_i$, is the same as the difference between T_0 and T_i , such that

$$(V_d)_i = T_0 - T_i = K(A_0 - A_i) \quad (47)$$

$$\left[\begin{array}{l} A_0 = A_0^{II} \quad A_i = A_i^{II} \quad (\text{region II}) \\ A_0 = A_0^{IV} \quad A_i = A_i^{IV} \quad (\text{region IV}) \end{array} \right]$$

It is very difficult to find the value of K theoretically, because it is affected by a variety of factors. It is determined by comparison between the simulation results by using this defect zone model and the experimental results by trial and error.

5. Results and discussions

Fig. 7 shows the measured valley profiles of the experimented specimens and the predicted valley profiles from the simulation results. Each vertical line of $x_i^{II} = 0.0$ in Fig. 7(a) and (c) is the straight line passing through the arc center and the ideal start point of arc, whereas the horizontal line of valley depth=0 corresponds to the after-machined flat-surface. Similarly, each vertical line of $\phi_i = 0$ in Fig. 7(b) and (d) is the straight line passing through the arc center and the ideal end point of arc, whereas the horizontal line of valley depth=0 corresponds to the after-machined arc-surface. To help in understanding the milled-surface geometry, the valley angles are shown as negative(-) values in this figure. The values of x_i^{II} or ϕ_i at the crossing point, where the valley profile intersects the horizontal line of valley depth=0, refer to the defect zone length or the valley angle respectively.

All curves in Fig. 7(a) show that the true depth of cut is gradually increasing compared to that of the already machined flat-surface when the tool is approaching the arc-surface. Fig. 7(b) also depicts that the true depth of cut is gradually decreasing compared to that of the already machined arc-surface when the tool is approaching the flat-surface. In summary, it can be presumed that the after-machined outer corner surface is rendered lower relatively near the arc, with a constant curvature in most of the arc-surface, and then becomes higher just before meeting the next flat-surface along the tool path. This presumption well matches the typical profile in Fig. 1(a). In the same way, the after-machined inner corner shape can be

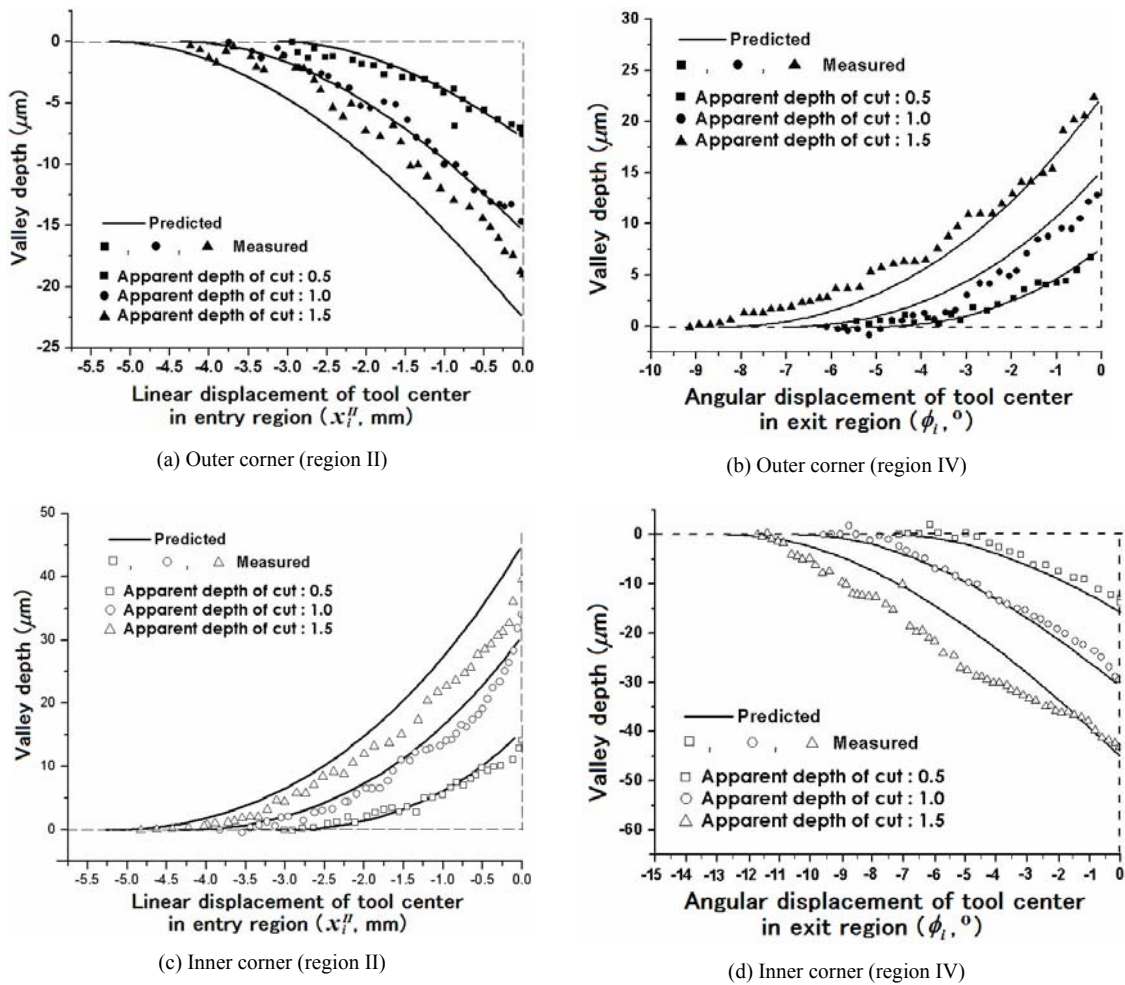


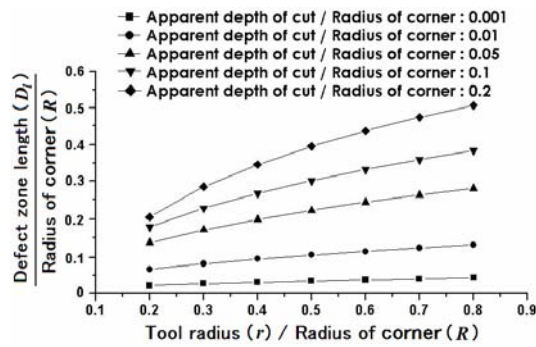
Fig. 7. Defect zone profile.

deduced by using Figs. 7(c) and (d), such that the flat-surface is rendered higher relatively near the arc, with also a constant curvature in the arc-surface, and then becomes lower just before meeting the next flat-surface. The difference between the typical profiles of the outer and inner corners is caused from the difference in the material removal per tooth values. Even though the same machining conditions are applied for both cases, the material removal per tooth can be different depending on the curvature of the tool path, because the feed rate on the workpiece surface is different from that of tool center.

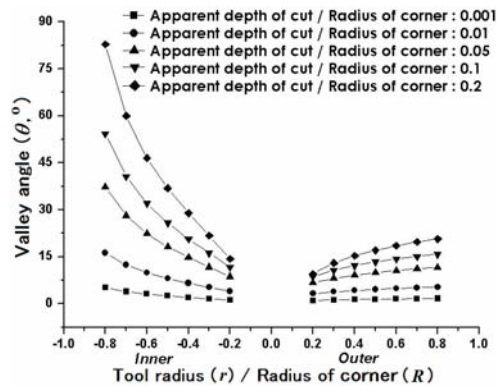
Even if there is some discrepancy between the measured values and predicted values, the predicted defect zone profiles provide the same tendency as the measured ones overall. It is presumed that the discrepancy is caused by the assumption for defining the

machining elasticity and the experimental errors in the end-milling and the measurement processes. All profiles describe that an increase in the apparent depth of cut makes the defect zone wider and deeper if the cutting conditions except the apparent depth of cut remain unchanged.

Through the modeling, it is expected that the defect zone is strongly affected not only by the apparent depth of cut, but also by the tool radius and the radius of corner, as can be ascertained from Fig. 8, in which the normalized Eqs. (3)-(6) including the parameters divided by the radius of corner are plotted. The defect zone lengths for both outer and inner corners remain the same under the same cutting conditions, so that curves in Fig. 8(a) can be valid for both cases. The valley angles for both cases are, however, governed by different equations. Fig. 8(b) includes the simula-



(a) Region II



(b) Region IV

Fig. 8. Effect of apparent depth of cut on defect zone length and valley angle (Simulation).

tion results of both cases where positive(+) and negative(-) values of the horizontal axis correspond to the case of outer and inner corner, respectively. As expected, the defect zone becomes wider when the ratio of tool radius : radius of corner increases. If the corner radius is given, the use of a bigger tool and larger apparent depth of cut would lead to wider and deeper defect zones on the corner surface. It is particularly critical when the tool is just before leaving the arc-surface and meeting another flat-surface in the case of inner corner. It is therefore recommended to design a corner with large radius and use a slender tool under cutting condition of the small apparent depth of cut.

6. Conclusions

Experimental and geometrical analyses have been performed to identify the location and size of a geometrically defected region in the side wall of corners during the flat end-milling process. In consequence,

the following conclusions have been drawn:

- If a corner surface is considered as a combination of a flat-surface, an arc-surface and another flat-surface patch, it has been found that the geometrically defected zones are always generated just before the tool is engaging the different surface patch.
- As a result, two defect zones exist in a corner surface, which are caused from the change of the material removal per tooth.
- It is also revealed that they are affected by the radius of corner, the tool radius and the apparent depth of cut directly.
- From the viewpoint of geometrical accuracy, it is more appropriate to machine a corner with a larger arc-radius using a slenderer end-milling tool under the cutting condition of smaller apparent depth of cut. None of them, however, can have values of infinity or zero. Thus, even if the size of the defect zone becomes smaller under the careful selection of cutting conditions, it cannot be eliminated or avoided.

Acknowledgment

This work was supported by research program 2006 of Kookmin University in Korea.

References

- [1] E. Budak and Y. Altintas, Peripheral milling conditions for improved dimensional accuracy, *Int. J. Mach. Tools Manu.*, 34 (7) (1994) 907-918.
- [2] J. G. Choi and M. Y. Yang, In-process prediction of the surface error using an identification of cutting depths in end milling operation by simulating surface, *J. of KSPE*, 15 (2) (1998) 114-123.
- [3] S. L. Ko, S. K. Lee and S. M. Bae, Study on the design of end mill geometry, *J. of KSPE*, 18 (8) (2001) 24-30.
- [4] S. K. Lee, and S. L. Ko, Analysis on the precision machining in end milling operation by simulating surface generation, *J. of KSPE*, 16 (4) (1999) 229-236.
- [5] S. H. Ryu, D. K. Choi and C. N. Chu, Optimal cutting condition in side wall milling considering form accuracy, *J. of KSPE*, 20 (10) (2003) 31-39.
- [6] J. Tlustý, S. Smith and C. Zamudia, New NC routines for quality in milling, *Annals of CIRP*, 39 (1)

- (1990) 517-521.
- [7] J. H. Yoon, M. S. Cheong and H. C. Lee, A study on transition of dimension error and surface precision in high speed machining of Al-alloy, *J. of KSMTE*, 9 (3) (2003) 96-102.
- [8] H. D. Cho and M. Y. Yang, A study on the prediction of tool deflection and precision machining in ball end milling process, *KSME Journal*, 16 (9) (1992) 1669-1680.
- [9] Y. H. Kim and S. L. Ko, Improvement of the accuracy in cornering cut using end mill, *KSME Journal*, Vol. 25/A (3) (2001) 399-407.
- [10] T. I. Seo and M. W. Cho, Tool trajectory generation based on tool deflection effects in flat-end milling process (I) -tool path compensation strategy, *KSME International Journal*, 13 (10) (1999) 738-751.
- [11] T. I. Seo and M. W. Cho, Tool trajectory generation based on tool deflection effects in flat-end milling process (II) -prediction and compensation of milled surface errors, *KSME International Journal*, 13 (12) (1999) 918-930.
- [12] K. Kim, Unavoidable geometric errors in the side walls of end-milled parts -flat surface-, *J. of Mech. Science and Tech.*, 21 (1) (2007) 48-56.
- [13] K. S. Lee and K. Kim, Unavoidable geometric errors in the side walls of end-milled parts -cylindrical surface-, *J. of Mech. Science and Tech.*, 22 (2008) 522-531.



Kun Sang Lee received his B. S. degree in Mechanical Engineering from Seoul National University, Korea, in 1982. He then received his Dipl.-Ing. and Dr.-Ing. degrees from Technical University of Berlin, Germany, in 1991 and 1993, respectively. Dr. Lee is currently a Professor at the School of Mechanical and Automotive Engineering at Kookmin University in Seoul, Korea. He serves as a Staff of the Korea Engineering Education Research Center. His research interests include precision machining, high energy beam material processing, and creative design methodology.



Kang Kim received his B. S. and M. S. degrees in Mechanical Design and Production Engineering from Seoul National University, Korea, in 1982 and 1984, respectively. He then received his Ph.D. degree from Purdue University, USA, in 1992.

Dr. Kim is currently a Professor at the School of Mechanical and Automotive Engineering at Kookmin University in Seoul, Korea. His research interests include material removal processes, and concurrent engineering.